

# Validated coastal flood modeling at Imperial Beach, California: Comparing total water level, empirical and numerical overtopping methodologies



T.W. Gallien

*Scripps Institution of Oceanography, University of California, San Diego, United States*

## ARTICLE INFO

### Article history:

Received 30 July 2015

Received in revised form 24 December 2015

Accepted 30 January 2016

Available online 4 March 2016

### Keywords:

Wave overtopping

XBeach

Coastal flooding

Hydrodynamic model

Bathtub model

Beach

## ABSTRACT

Flood extent field observations collected during a winter storm ( $H_s \sim 1.8$  m,  $T_p \sim 14$  s) coinciding with a spring high tide are used to evaluate the accuracy of static ('bathtub') and hydrodynamic coastal flood modeling methodologies. Static models rely on empirically calculated wave setup or runup and simply compare total water level (TWL) to land elevation. The dynamic model resolves temporally variable overtopping rates, overland flow, urban features and storm system drainage. SWAN, a numerical wave model, transformed deep water buoy spectra to the nearshore. Static TWLs were calculated using SWAN output and an empirical runup model. Numerical (XBeach) and Empirical (EurOtop) overtopping models parameterized with survey data and SWAN bulk wave statistics estimated temporally variable overflow rates along representative transects for overland flow model input. XBeach model mode (hydrostatic, nonhydrostatic), boundary depth and random realizations significantly affected overtopping rates. Nonhydrostatic mode estimated order of magnitude larger overflow volumes suggesting the importance of incident waves, particularly in near threshold conditions. Boundary depth and random realizations varied overflow rates approximately fourfold. Field observations showed static TWL models performed poorly, maximum runup substantially overestimated flood extent and setup predicted no flooding. All dynamic models reasonably predicted flood extent despite significant overflow volume differences. Backshore topography and flow dynamics are important flood extent controls. Accurate near threshold coastal flood predictions require dynamic overland flow modeling parameterized with temporally variable overtopping estimates and site specific beach and backshore topography.

© 2016 Elsevier B.V. All rights reserved.

## 1. Introduction

### 1.1. Background

Globally, coastal flooding represents a significant humanitarian and socioeconomic hazard, 20 million people live under current high tide levels and 200 million under storm tide levels (Nicholls, 2010). The recent IPCC report suggests global mean sea levels will rise 36–71 cm by 2100 under the RCP4.5 moderate emissions scenario (Church, 2013). Concerningly, mean higher high water (MHHW) and mean high water (MHW), peak levels that drive coastal flooding, show significant upward trends in many locations (Flick et al., 2003; Mawdsley et al., 2015). Relatively modest sea level rise (i.e., 0.50 m) will significantly increase flood frequencies (Hunter, 2012). For example, Sweet and Park (2014) show that 'tipping points', i.e., flooding over 0.5 m above MHHW levels will be reached by 2050, while

Tebaldi et al. (2012) suggest that the 100 year coastal flood will become annual to decadal events for much of the United States.

Coastal flood vulnerability is evaluated using two modeling methodologies; static (also known as bathtub, equilibrium or planar surface projection models), and hydrodynamic models (e.g., BreZo, DIVAST, TELEMAC-2D, TUFLOW) that solve the equations of mass and momentum. Static methods simply compare water and land elevations and assume that flooding occurs instantaneously when water levels exceed backshore elevations. Static models (e.g., Heberger et al., 2009; Climate Central, 2015; NOAA, 2015) are widely used to assess regional sea level rise vulnerability and have been shown to substantially overpredict coastal flooding in low elevation backshores (Bernatchez et al., 2011; Gallien et al., 2011, 2014). Two-dimensional (2D) hydrodynamic models accurately simulate long wave dynamics and overland flow (e.g., Bates et al., 2005; Brown et al., 2007; Purvis et al., 2008; Dawson et al., 2009; Knowles, 2009; Martinelli et al., 2010; Smith, 2012; Wadey et al., 2012). However, temporally and spatially variable overtopping, fundamental to accurate coastal flood prediction, are rarely included in hydrodynamic

E-mail address: [tgallien@ucsd.edu](mailto:tgallien@ucsd.edu) (T. Gallien).

flooding models. Overtopping flows are a significant deficiency in coastal flood modeling efforts (Hubbard and Dodd, 2002; Hunt, 2005; Brown et al., 2007), and prioritized as a critical future research area (Wadey et al., 2012).

A simplistic method for representing overtopping flows uses a calculated total water level (TWL) based on Stockdon et al. (2006)  $R_{2\%}$  (e.g., FEMA, 2004; Heberger et al., 2009) or maximum water level output from numerical models such as XBeach (e.g., Barnard et al., 2014). TWL models are applied using a static (bathtub) method, projecting the maximum water level over the backshore and suffers identical deficiencies as typical static modeling, significantly overpredicting backshore flooding (Bates et al., 2005; Gallien et al., 2014). Few studies have attempted to resolve temporally and spatially variable overtopping flows and fewer still incorporate validation data. Laudier et al. (2011) investigated beach overtopping and lagoon filling in Central California and suggested that empirical overtopping models overestimated total overtopped volume. Gallien et al. (2014) used empirical overtopping estimates as source point input into an overland flow solver and showed good agreement with validation data, though some overprediction was observed. Cheung et al. (2003) and Lynett et al. (2010) presented numerical overtopping models along with qualitative validation data (e.g., high water marks or

levee damage), however in the case of Lynett et al. (2010), empirical and numerical estimates differed by an order of magnitude. Le Roy et al. (2014) coupled nearshore wave and phase resolving nonlinear shallow water (NLSW) models to hindcast overtopping flooding, however variable quality high water marks supported only qualitative validation. Numerous studies show the critical need for field validation data (e.g., Battjes and Gerritsen, 2002; Poulter and Halpin, 2008; Reeve et al., 2008; Anselme et al., 2011; Gallien et al., 2012).

XBeach (Roelvink et al., 2009) is a process based flow and sediment transport model that considers infragravity and incident wave forcing. XBeach solves a time dependent wave action balance that forces a Generalized Lagrangian Mean (GLM) formulation of the nonlinear shallow water equations (Roelvink et al., 2009). A one-layer, nonhydrostatic pressure correction (Zijlema and Stelling, 2008) enables short wave surface elevation variation. For a complete model description see Roelvink et al. (2009) and Smit et al. (2010). XBeach has been used primarily to model erosion and overwash during storm events (e.g., Roelvink et al., 2009; McCall, 2010; Splinter and Palmsten, 2012; McCall, 2013). Here, uncalibrated XBeach is used to numerically estimate temporally variable overtopping volumes on a sandy beach during a winter storm event. Waves, water level, flood modeling and observations are described in Section 2.

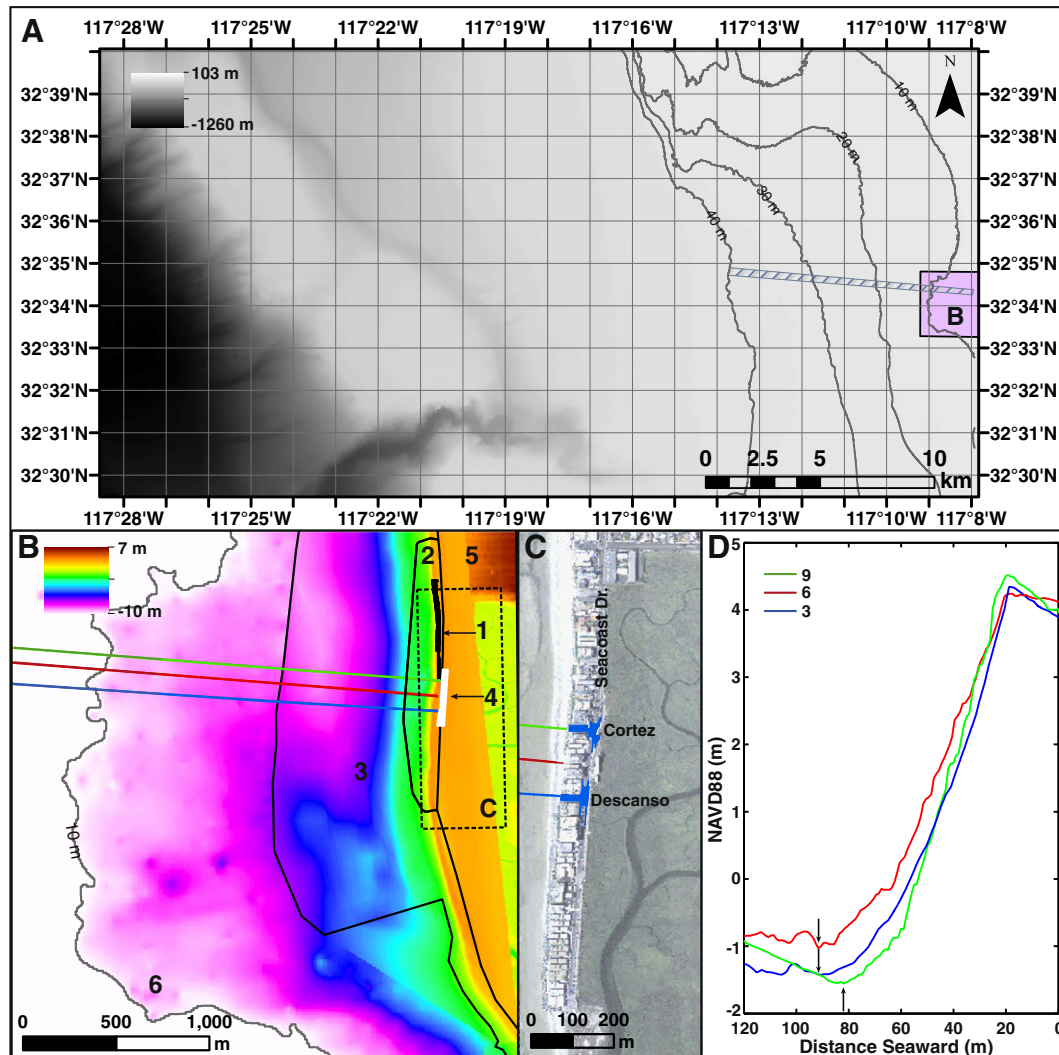


**Fig. 1.** Imperial Beach Site and Data Sources. (A) Bathymetry with XBeach transects envelope (striped area) and 10–40 m isobaths. (B) Nearshore data with 10 m isobath. XBeach transects 3, 6 and 9 are shown as solid blue, red and green lines, respectively. (C) Flood modeling domain, transects and observed flood extent (blue). (D) Foreshore transects, black arrows denote slope toes. Numerals correspond to geospatial data priorities in Table 1. All data in NAVD88 m unless otherwise shown.

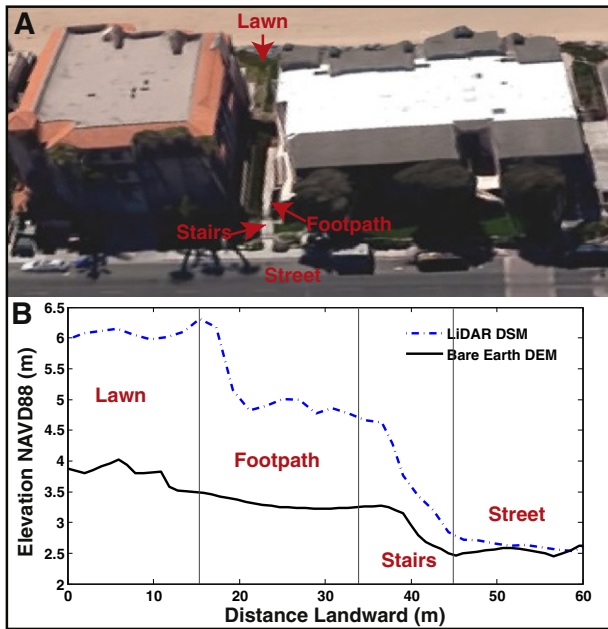


**Fig. 2.** Site Specific Topography. (A) Google Earth back beach topography showing terrain features between houses. (B) LiDAR DSM and bare earth DEM comparison along a transect between structures where bare earth DEM is oversmoothed.

Results are presented in Section 3. Modeling methodology, boundary conditions and site specific data discussions (Section 4) are followed by a summary (Section 5).

## 2. Methods

### 2.1. Site description

Imperial Beach, California is a low-lying southern California coastal community located between San Diego and the US–Mexico border. The southernmost portion of the city, Fig. 1C, is a sand spit backed by the Tijuana Estuary that frequently floods. In September and October, 2012 344,000 m<sup>3</sup> of sand were placed on the beach from Cortez Avenue south adding approximately 60 m of subaerial beach. The nourishment profile steepened, retreated and developed wave cut crowns (Ludka et al., 2015).

### 2.2. Flood event description

On January 30, 2014 winter storm waves ( $H_s \sim 1.8$  m,  $T_p \sim 14$  s,  $D_p \sim 280^\circ$ ) coinciding with a spring high tide, 2.1 m North American Vertical Datum of 1988 (NAVD88), overtopped Imperial Beach’s southern reach, flooding Cortez, Descanso and Seacoast Drive. The field team arrived at 14:30 coordinated universal time (UTC) and observed overtopping and minor flooding. Overtopping

peaked around 16:00 UTC and occurred intermittently until approximately 18:15 UTC. A hand dolly fitted with a Real Time Kinematic (RTK) GPS receiver mapped the maximum flood extent.

### 2.3. Digital elevation model topographic and bathymetric datasets

A digital terrain model (DTM) from approximately 33 km offshore and 500 m landward of the beach was constructed in World Geodetic System 1984 (WGS84) and NAVD88 m (Fig. 1) using offshore bathymetry from NOAA Geophysical Data Center (Carignan et al., 2012) and bare earth California Coastal Conservancy topography from NOAA digital Coast (<http://coast.noaa.gov/dataviewer>). The bare earth digital elevation model (DEM) exhibits a highly smoothed landward sloping surface inconsistent with the site (Fig. 2). An alternate LiDAR digital surface model (DSM) that did not remove structures was consistent with the observed back beach region. DSM elevation data between houses were used to supplant incorrect bare earth DEM elevations. Beach crest elevations were surveyed immediately before high tide, comprehensive beach topography was surveyed at the following low tide. Nearshore bathymetry from 0 to –8 m NAVD88 m was surveyed two weeks prior to the overtopping event. Beach to pography was blended with nearshore bathymetry, bare earth topographic data and offshore bathymetry. Table 1 shows the data sources, in order of priority, used to construct the DTM.

### 2.4. Wave modeling

Six minute water levels were obtained from the nearest open coast tide gauge, La Jolla 9410230, approximately 40 km north and applied as offshore boundary conditions for all models. Deep water boundary condition half-hourly frequency directional spectra (CDIP buoy 191, <http://cdip.ucsd.edu>) were calculated using the maximum entropy method (64 frequency, 360 directional bins) and propagated shoreward using SWAN (Booij et al., 1999). The 33 × 20 km (660 × 400) simulation domain, gridded at ~50 m spacing, was carefully chosen to preserve wave properties in the region of interest, i.e. boundary shadowing and grid resolution effects were negligible. An eight hour non-stationary simulation (11:00–19:00 UTC) output significant wave height ( $H_s$ ), peak period ( $T_p$ ), peak direction ( $D_p$ ) and directional spread ( $\sigma_e$ ) at 6 minute intervals at 40 m, 10 m the slope toe (~–1 m NAVD88) along three representative cross-shore transects (Fig. 3). The first hour of output was discarded.

### 2.5. TWL estimates

Total water levels were estimated using Stockdon et al. (2006) setup ( $\bar{\eta}$ ) and runup,  $R_{2\%}$ ,

$$\langle \bar{\eta} \rangle = 0.35\beta(H_0L_0)^{0.5} \tag{1}$$

$$R_{2\%} = 1.1 \left( 0.35\beta(H_0L_0)^{0.5} + \frac{[H_0L_0(0.563\beta^2 + 0.004)]^{0.5}}{2} \right) \tag{2}$$

**Table 1**  
Geospatial data. Resolution given is point spacing along crest line<sup>1</sup>, 5 m transects<sup>2</sup> and 100 m ransects<sup>3</sup>.

Priority	Location	Description	Source	Date	Resolution (m)	VRMSE (cm)
1	Beach crest	Dolly survey	Scripps	01-30-14	0.8 <sup>1</sup>	2
2	Upper beach	ATV survey	Scripps	01-30-14	0.6 <sup>2</sup>	3
3	Beach to –8 m	ATV, dolly, jet ski	Scripps	01-14-14	0.8 <sup>3</sup>	3
4	Backbeach	LiDAR DSM	Scripps	04-08	2	10
5	Land/Estuary	Bare earth DEM	CA Coastal Cons.	10-09 to 08-11	1	10
6	Offshore	1/3 arc second DEM	NOAA NDGC	Various	1–10	10–100

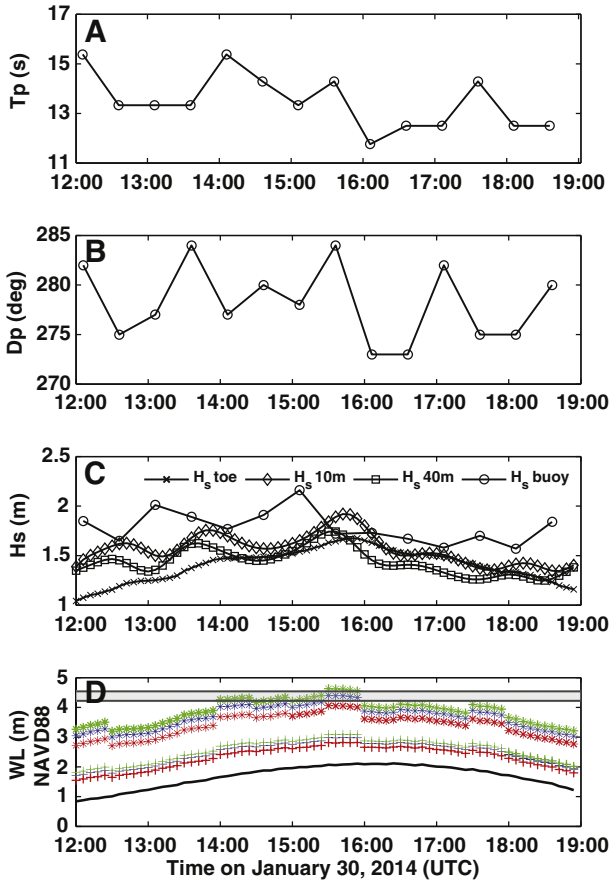


Fig. 3. Wave and water level data. (A) Offshore peak period, (B) peak direction, (C) significant wave height, (D) water level (black line) and TWL estimates for  $R_2\%$  runup (\*) and setup (+). Transect colors as described in Fig. 1. Gray band shows minimum and maximum beach crest.

where  $\beta$  is the slope,  $H_0$  is the deep water significant wave height,  $L_0$  is the deep water wave length. SWAN significant wave height estimates in 40 m depth were linearly reverse shoaled for calculating Stockdon TWLs.

## 2.6. Dynamic water level and overtopping estimates

Maximum wave runup elevation and overtopping volumes were estimated over a seven hour period (12:00–19:00 UTC) using EurOtop (Pullen et al., 2007) and XBeach (Roelvink et al., 2009). EurOtop was developed for dike structures and relies on bulk wave parameters and beach geometry to estimate average overtopping rates. Although EurOtop is intended for runup and overtopping of structures it has been used to estimate beach and dune overtopping volumes (e.g., Martinelli et al., 2010; Laudier et al., 2011; Gallien et al., 2014). The probabilistic EurOtop formulation for  $\xi_{m-1,0} < 5$  is,

$$\frac{q}{\sqrt{gH_{m0}^3}} = \min(a, b)$$

$$a = \frac{0.067}{\sqrt{\tan \alpha}} \gamma_b \xi_{m-1,0} \exp\left(-4.75 \frac{R_c}{\xi_{m-1,0} H_{m0} \gamma_b \gamma_f \gamma_\beta \gamma_v}\right) \quad (3)$$

$$b = 0.2 \exp\left(-2.6 \frac{R_c}{H_{m0} \gamma_f \gamma_\beta}\right)$$

where  $q$  is the mean overtopping rate per unit length,  $g$  represents gravity,  $\alpha$  is slope angle,  $R_c$  is the freeboard,  $H_{m0}$  is the significant

wave height at the structure toe,  $\gamma_b$  is the berm influence factor,  $\gamma_f$  is the roughness influence factor,  $\gamma_\beta$  is the oblique wave attack factor,  $\gamma_v$  is the vertical wall influence factor (Pullen et al., 2007). All reduction parameters were assumed to be unity. The TAW (2002) formulation relies on a breaker parameter  $\xi_{m-1,0}$  that characterizes the wave breaking condition (i.e., breaking, non-breaking) and is given as,

$$\xi_{m-1,0} = \frac{\tan \alpha}{\sqrt{\frac{H_{m0}}{L_{m-1,0}}}} \quad (4)$$

where  $L_{m-1,0} = gT_{m-1,0}^2/2\pi$  and  $T_{m-1,0} \approx T_p/1.1$  (Pullen et al., 2007). Wave overtopping volumes were estimated using  $T_{m-1,0}$  calculated from 30 minute buoy data, six minute SWAN significant wave height output at the slope toe and beach topography from the DTM.

Although Stockdon calculates runup and EurOtop estimates overtopping, overtopping is a function of runup and would presumably include identical physical dependencies. The dependency in Stockdon is the product of  $H_0 L_0$  while EurOtop (Eq. (4)) depends on the quotient,  $H_{m0}/L_{m-1,0}$ .

XBeach was run in one-dimensional (1D) profiles in hydrostatic and nonhydrostatic mode along three transects. Spatially variable 1D grids were optimized using the XBeach Matlab toolbox 'xb\_grid\_xgrid'. Hydrostatic gridding resulted in approximately 120 and 270 cells for offshore XBeach boundary conditions in 10 m and 40 m depths, respectively. Nonhydrostatic gridding resulted in approximately 600 and 2900 cells for the 10 and 40 m boundaries, respectively. SWAN bulk wave parameters and La Jolla water levels were used as offshore boundary conditions. Sediment transport and morphology were set to 0 (off). Recent studies impose XBeach boundaries in relatively shallow, 8–15 m, depths (e.g., Barnard et al., 2014; Stockdon et al., 2014). In the present case,  $\sim 40$  m satisfies the ratio of group celerity to wave celerity ( $n \sim 0.8$ ,  $kd \sim 1$ ) recommended on the XBeach forum (McCall, 2013). Ten XBeach realizations using 10 and 40 m SWAN outputs ( $H_s$ ,  $T_p$ ,  $\sigma_x$ ) were run in both hydro- and non-hydrostatic modes along three transects (120 total simulations). Wave overtopping volumes were estimated at 1 Hz from water height and velocities immediately shoreward of the maximum beach elevation (arrow, Fig. 4C) for each transect. Hydrostatic run times were approximately 90 and 140 s for 10 and 40 m. Nonhydrostatic run times were approximately 600 and 3600 s for 10 and 40 m, respectively.

## 2.7. Flood modeling

Overland flow and drainage from the storm water system was modeled using BreZo, a two-dimensional Godunov type finite volume model that solves the nonlinear shallow water equations. A constrained Delaunay triangulation was generated using Triangle (Shewchuk, 1996) consisting of 8234 triangles representing the 1200 m  $\times$  380 m domain along Seacoast Drive. A spatially variable mesh, gradating from  $\sim 25$  m offshore to  $\sim 3$  m along beaches and roads where flooding occurred. A minimum of three cells across were used to resolve street flows. Wave overtopping volumes were introduced to the overland flow model at multiple locations to consider source point number, distribution and position effects.

Surface streets are gravity drained into the estuary via the storm water system and are represented by point sinks in the overland flow model using a weir equation;

$$Q_{ss} = \frac{2}{3} C_d \left(\frac{2}{3} g\right)^{1/2} L H^{3/2} \quad (5)$$

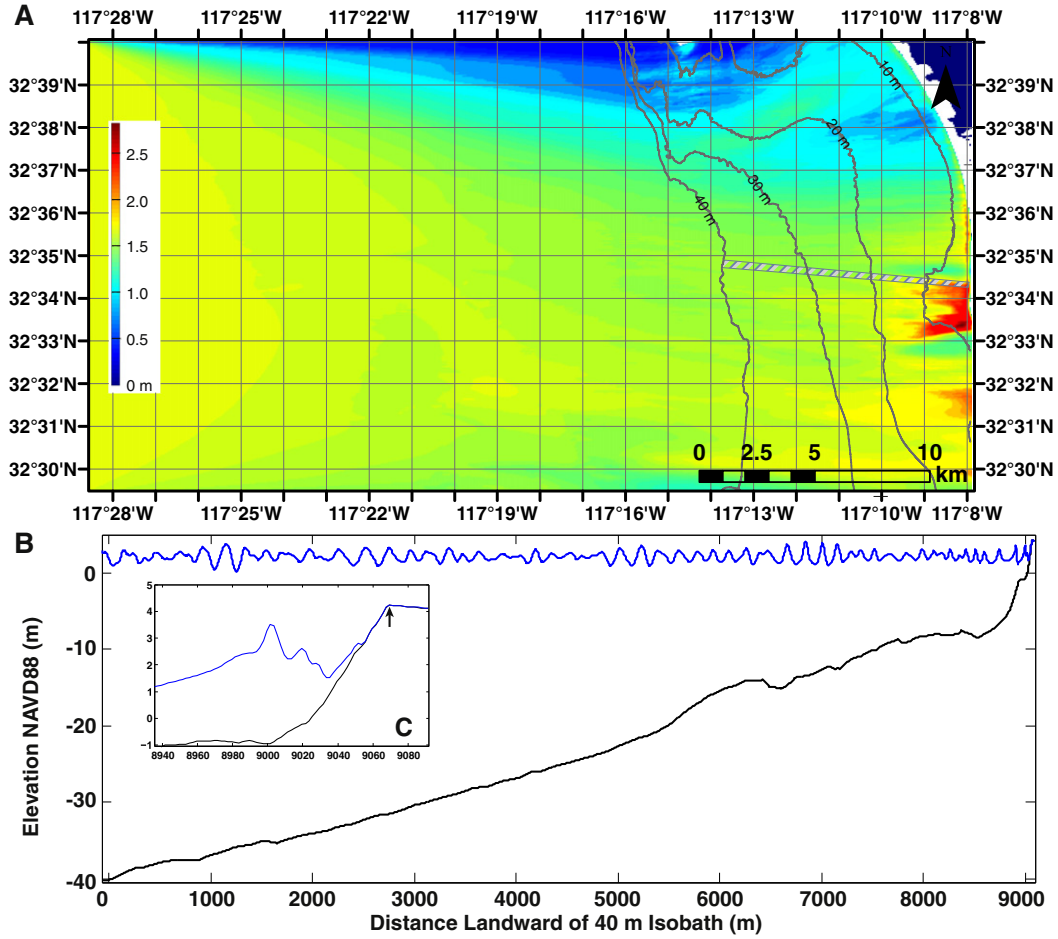


Fig. 4. (A) SWAN significant wave height output at 16:00 UTC with XBeach transect envelope (striped area) and 10–40 m isobaths, (B) XBeach 40 m boundary, nonhydrostatic water level (blue) at 16:00 UTC along transect 6. Inset (C) beach detail, arrow shows nearshore overtopping estimate location.

where  $Q_{ss}$  represents flow into the storm sewer,  $C_d$  is the coefficient of discharge,  $L$  is the drain opening width and  $H$  is the water depth.

Flood modeling was performed in serial on a Dell T3600 workstation with an Intel quad core 3.6 GHz processor. A 7 hour simulation, resolving the rising, peak and ebbing tide required approximately 5 min of CPU time. A 0.2 s time step satisfied the Courant–Friedrichs–Levy (CFL) criterion. The model was first applied using a tidal boundary condition to consider the possibility of ocean or bay-side tidal flooding. Consistent with observations, no tidal flooding occurred. All flooding was caused exclusively by ocean-side overtopping.

2.8. Fit measures

Three fit metrics describe the goodness-of-fit between predicted and observed flood extents. The coefficient of areal correspondence,  $F_A$  (Taylor, 1977), shows the agreement between prediction and

observation and is defined as the intersection of predicted and observed flood extents divided by the union of the predicted and observed flood extent,

$$F_A = \frac{E_p \cap E_o}{E_p \cup E_o} \tag{6}$$

where  $E_o$  and  $E_p$  represent the observed and predicted flood extent, respectively. Perfect agreement would result in  $F_A = 1$ . Underprediction,  $F_{UP}$ , is characterized by the fraction of flooded area observed, but not predicted.

$$F_{UP} = \frac{E_o - E_p \cap E_o}{E_p \cup E_o} \tag{7}$$

Table 2

Transect data, Stockdon runoff and XBeach average maximum onshore water level results. All dimension in meters, except slope,  $\beta$  (non-dimensional),  $z_{max}$  is the maximum beach elevation. Standard deviations are shown in parentheses.

Transect	$\beta$	$z_{max}$	$R_{2\%}$	10 m hydro	10 m nonhydro	40 m hydro	40 m nonhydro
3	0.117	4.34	4.54	4.49(0.06)	4.79(0.10)	4.12(0.18)	4.65(0.04)
6	0.096	4.24	4.19	4.45(0.07)	4.71(0.18)	4.09(0.19)	4.51(0.07)
9	0.132	4.52	4.79	4.60(0.05)	4.81(0.11)	4.15(0.26)	4.67(0.06)

**Table 3**  
 Overtopping model results. EurOtop results are deterministic. Each XBeach model was run 10 times for each transect, the mean and standard deviations (in parentheses) are shown. Overtopping time ( $T_{or}$ ) is considered for flows over 1 l/s/m.  $q_{max}$  and  $V_{total}$  are runs nearest to the mean.  $V_{total}$  is scaled by the representative reach length of each transect.

Model	Mode	Depth (m)	Transect	$q_{max}$ l/s/m	$Q_{tot}$ (l/m)	$V_{total}$ (m <sup>3</sup> )	$T_{or}$ (s)	$Q_{avg}$ (l/m/s)
EurOtop		~1	3	25.4	162,180	12,164	19,080	8.5
		~1	6	11.5	64,900	3,894	14,760	4.4
		~1	9	32.5	193,860	18,147	19,440	10.0
XBeach	Hydrostatic	10	3	433	4,531(2380)	387	57.4(14.4)	76.4(32.2)
		10	6	600	12,827(2908)	673	282(49)	46.3(10.6)
		10	9	158	1,263(1311)	97	20(12)	50.6(31.0)
XBeach	Nonhydrostatic	10	3	2,393	35,171(7626)	2,901	337(28)	102(16)
		10	6	1,866	34,124(5470)	2,028	361(41)	95(15)
		10	9	1,043	6,042(3126)	573	63(24)	97(38)
XBeach	Hydrostatic	40	3	*	*	*	*	*
		40	6	*	*	*	*	*
		40	9	*	*	*	*	*
XBeach	Nonhydrostatic	40	3	831	8,595(6222)	645	113(19)	78(35.5)
		40	6	685	7,471(3802)	439	192(66)	37.5(11.1)
		40	9	290	2,142(1459)	204	54.4(21.5)	364(13.6)

\* Indicates zero or insignificant overtopping.

$F_{UP} = 0$  corresponds to no underprediction. Lastly, overprediction,  $F_{OP}$ , characterizes the fraction of flooded area predicted but not observed.

$$F_{OP} = \frac{E_P - E_P \cap E_O}{E_P \cup E_O} \quad (8)$$

and  $F_{OP} = 0$  corresponds to no overprediction. Superior models will maximize  $F_A$  and minimize both  $F_{UP}$  and  $F_{OP}$ .

### 3. Results

#### 3.1. Runup and overtopping

Table 2 shows Stockdon  $R_{2\%}$  runup and average maximum onshore water levels, the maximum free surface elevation measured at the beach crest, for all XBeach realizations. Slope dependency is observed in both empirical and numerical results, maximum runup increases with beach foreshore steepness but is considerably stronger in Stockdon. Stockdon  $R_{2\%}$  varies by 60 cm across the three transects while XBeach average maximum onshore water level elevations vary less than 16 cm. Each XBeach model considers 10 realizations, maximum water level estimates for all realizations and transects (120 total) varied from ~3.8 to 5 m. Model mode (i.e., hydrostatic, nonhydrostatic) and boundary depth significantly

effect XBeach water level estimates (Table 2). Across all transects, hydrostatic models estimated substantially lower (21–53 cm) runup than corresponding nonhydrostatic results. Lower average maximum water levels (14–45 cm) were observed using the deeper 40 m boundary.

XBeach boundary depth (10 or 40 m) and modeling mode (hydrostatic or nonhydrostatic) significantly affect overtopping estimates. Nonhydrostatic modeling increased transect overtopping rates and

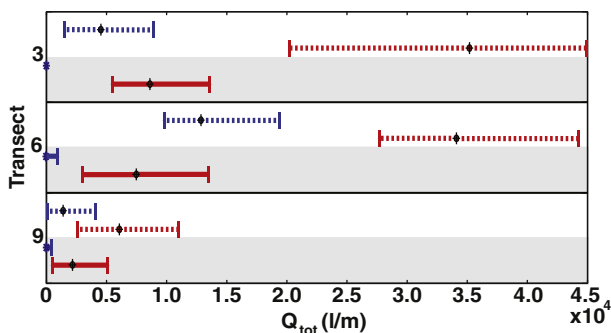


**Fig. 5.** Summary of all XBeach overtopping realizations for each transect. 10 m boundary (white background, dashed lines), 40 m boundary (gray background, solid lines), hydrostatic (blue bars), nonhydrostatic (red bars). Realization mean is shown by circle and cross, vertical bars represent minimum and maximum of 10 runs. Asterisk is used when 80% or more of realizations predicted zero overtopping.

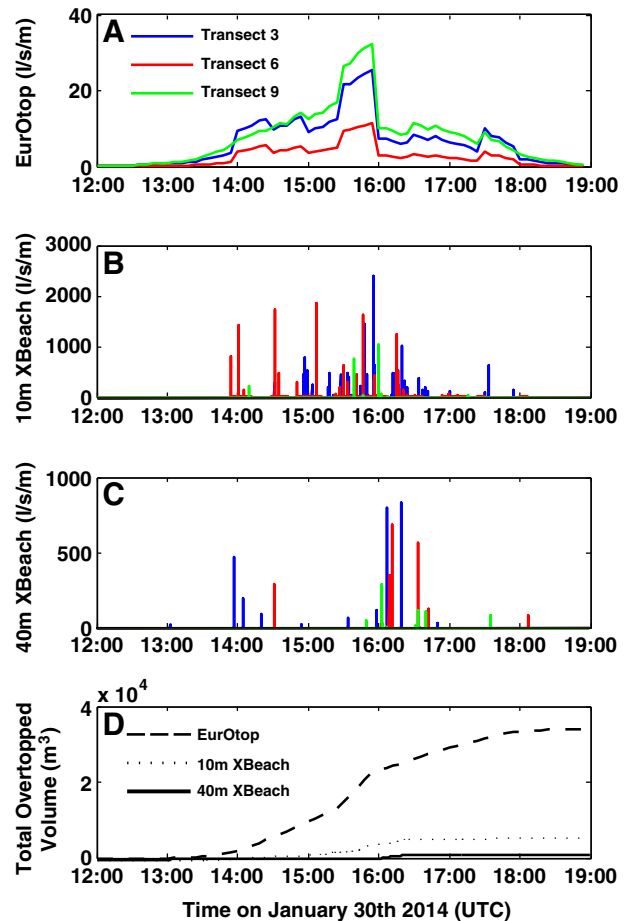


**Fig. 6.** Dynamic overtopping rates for (A) EurOtop, (B) 10 m XBeach, (C) 40 m XBeach and (D) cumulative total overtopped volume.

**Table 4**

Flood models and statistics. All heights are in centimeters.

Model	$F_A$	$F_{OP}$	$F_{UP}$	$h_{avg}$	$h_{max}$	$h_{Cortez}$
Stockdon $R_{2\%}$	0.13	0.87	0	–	–	–
Stockdon SU	0	0	1	–	–	–
EurOtop	0.64	0.34	0.02	9.5	27.3	2.4
10 m XBeach	0.67	0.29	0.04	10.9	25.1	9.9
40 m XBeach	0.71	0.15	0.14	6.9	18.9	5.3

volumes (Table 3, Fig. 5) and predicted overtopping for all realizations (60 total). Hydrostatic modeling predicted overtopping for nearly all 10 m realizations (Fig. 5, white bands, dashed blue lines) but only 16% (5/30) of the 40 m realizations (Fig. 5, gray bands, blue asterisks).

XBeach predicts impulsive overtopping rates while EurOtop predicts average overtopping rates (Fig. 6), accordingly XBeach predicts substantially higher maximum overtopping rates ( $q_{max}$ ) while EurOtop predicts orders of magnitude higher overtopped ( $Q_{tot}$ ) and total ( $V_{total}$ ) volumes. For example, on transect 3 EurOtop predicts a maximum rate of 25.5 l/s/m and a total overtopped volume of  $1.6 \times 10^5$  l/m, nonhydrostatic 40 m XBeach predicts maximum rates and volumes of 831 l/s/m and 8595 l/m.

EurOtop's exponential formulation always predicts overtopping, if flows over 1 l/s/m are considered, EurOtop predicts overtopping flows for over four hours while XBeach only predicts 1–5 min total overtopping time (Fig. 6). If average overtopping rates are considered i.e., total overtopped volume ( $Q_{tot}$ ) divided by the overtopping time ( $T_{ot}$ ) order of magnitude differences are observed. EurOtop and nonhydrostatic XBeach realizations at 10 and 40 m depths nearest to the mean overtopping rate were chosen as input to the hydrodynamic flood model.

### 3.2. Static and hydrodynamic flood modeling

Five total flood models are considered (Table 4); two static water levels, Stockdon setup and  $R_{2\%}$  (Fig. 7A), and three hydrodynamic

models using EurOtop, XBeach 10 m nonhydrostatic, and XBeach 40 m nonhydrostatic overtopping estimates (Fig. 7B–D, respectively). Static TWL flood prediction is poor; Stockdon setup (not shown) predicts no flooding ( $F_A = 0$ ,  $F_{UP} = 1$ ) while  $R_{2\%}$  extensively overpredicts ( $F_A = 0.13$ ,  $F_{OP} = 0.87$ ). Flood models parameterized with nonhydrostatic 40 m XBeach (Fig. 7D) were most consistent with areal extent ( $F_A = 0.71$ ), flood arrival time and qualitative depth observations. From an areal extent perspective, all hydrodynamic models perform similarly ( $F_A \sim 0.7$ ) despite order of magnitude differences in overtopped volume inputs. However, flow characteristics differ substantially. EurOtop overtopping is a long, slow filling event, maximum water levels near the beach are 2.4 cm (Table 4,  $h_{Cortez}$ ) compared to higher levels, 5–10 cm, for impulsive (XBeach) overtopping. Flow vector analysis suggests that constant low level EurOtop flows are constrained by the curb, spread along gutters and discharge through the storm drains (Fig. 7B). Conversely, in impulsive flooding events water flows down Descanso and Cortez streets and surges across the curb into the estuary.

### 3.3. Overtopping input locations and spacing

Wave overtopping volume time series are input to the overland flow model as source points at various long and cross-shore locations. In hard structure flood modeling, grid cells or mesh edges are aligned with infrastructure (i.e., sea walls) and overtopping volumes are introduced along these features (e.g., Prime et al., 2015). Beaches, however, include fine scale, sub-meter topography (e.g., cusps, scarp), representing meshing challenges similar to those reported by Tsubaki and Fujita (2010) and Gallien et al. (2011). A computationally efficient mesh prohibits exact representation of the beach crest, some mesh cells will interpolate across the high elevation crest (Fig. 8). Flow vector analysis shows grid cells that interpolate across the high elevation feature may incorrectly slope and route overtopped water seaward. Input point cross-shore placement relative to beach crest, mesh edges and cell slope become important. Various

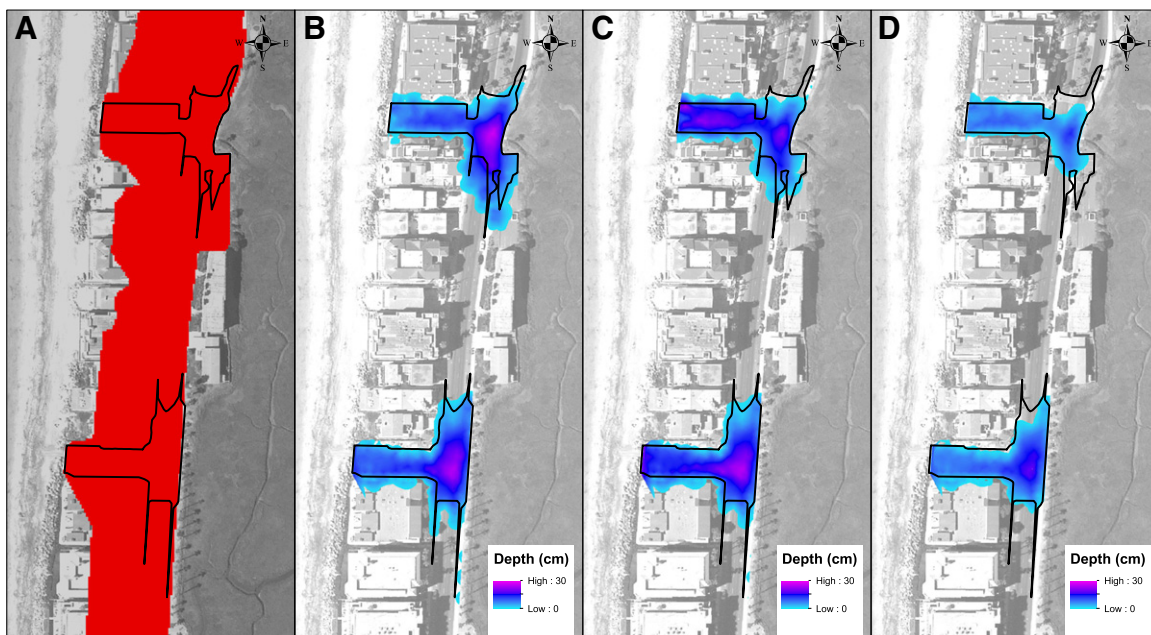


**Fig. 7.** Static (A) Stockdon  $R_{2\%}$  TWL and dynamic (B) EurOtop, (C) 10 m XBeach, (D) 40 m XBeach flood predictions and field validation data (black line). Stockdon setup predicted no flooding and is not shown. Static models do not predict flooding depth, extent is shown in red.

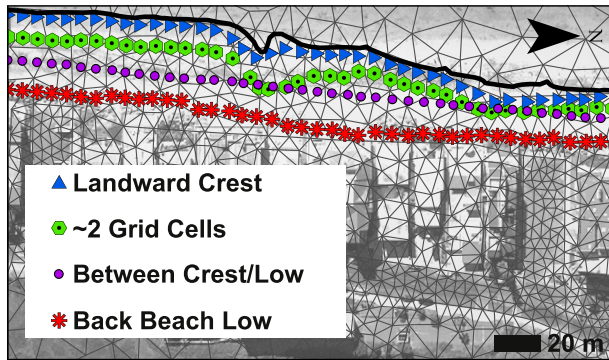


**Fig. 8.** Model mesh and source locations. Black curve is the maximum beach elevation. Source locations: landward of the maximum beach crest (blue triangles, Table 5, Trial 1); ~2 grid cells landward of the maximum beach crest (green hexagons, Table 5, Trial 2); along a line approximately halfway between the crest and back beach low elevation contour (purple circles, Table 5, Trial 3); low elevation back beach contour (red asterisks, Table 5, Trial 4).

cross-shore source locations are considered (Fig. 8 and Table 5, Trials 1–4); aligned immediately landward the DTM maximum beach elevation contour, two grid cells landward of the maximum beach elevation, along a line approximately halfway between the maximum beach elevation and low elevation contour landward of the crest but seaward of the urbanization and finally, the low elevation beach contour. All trials produced nearly identical results except when input points were aligned with the DTM maximum beach elevation contour (Trial 1).

#### 4. Discussion

Backshore flooding results from dynamic wave runup and overtopping processes. Temporally variable overtopping volume models were superior to TWL methods. All static models are incapable of resolving dynamic overtopping flows. Simple Stockdon  $R_{2\%}$  TWL models substantially overpredicted flood extent. Conversely, setup TWL predicted no backshore flooding. Continued reliance on static methods and corresponding poor prediction undermines coastal flood risk management efforts.

Interestingly, flood extents were similar for all dynamic overtopping models despite orders of magnitude difference in overtopped volume, suggesting that backshore topography and flow dynamics are primary flood extent controls.

Typically, XBeach is applied in a single deterministic run and offshore boundaries are imposed at instrumentation locations

(e.g., Stockdon et al., 2014) or set depths (e.g., Barnard et al., 2014). Random realizations of otherwise identical XBeach runs yielded significant variation in overtopping estimates, particularly when runup elevations are similar to maximum beach elevations. Although relative standard deviations decreased with increasing freeboard exceedance and subsequent overtopping events, overflow discrepancies may result in fundamentally different flooding predictions, particularly in areas with estuary side sea walls that retain overtopped volumes (e.g., Gallien et al., 2014). Alternative offshore boundaries (10 and 40 m) varied average maximum water levels by 14–45 cm and overtopping estimates approximately fourfold, suggesting that infragravity energy generated at the XBeach boundary varies significantly with boundary depth.

Long and cross-shore source locations must be considered for accurate flood predictions. Sources should be distributed along the beach, sufficiently seaward of urban features and landward of beach crest such that overtopped water correctly routes across the beach surface (Table 5, Trials 2–9). In this case, longshore spacings of 30 m or less appropriately routed water across local topographic depressions and into the backshore. Cross-shore locations coinciding with seaward sloping grid cells incorrectly routed overtopped volume and should be avoided (Table 5, Trial 1). Sparse longshore (in this case, 80 m) or excessively landward input points (Table 5, Trial 11) caused significant overprediction.

Generally, bare earth LIDAR based DTMs are recommended for routing overland flows (Sanders, 2007). However, in steep and rapidly variable terrain common to urbanized sand spits, structure removal may oversmooth high backbeach elevations. Fig. 2 shows the difference between the bare earth DTM and a LIDAR DSM, differences of ~2 m are observed between the two datasets between buildings. This highlights the critical site knowledge required to accurately model rapidly variable, urbanized backshore terrain.

#### 5. Conclusions

A nested modeling methodology is used to predict wave overtopping flooding. SWAN transformed offshore buoy data to the nearshore where XBeach estimated wave overtopping volumes as input to a nonlinear shallow water solver for backshore flood prediction. Model results are compared to traditional static TWL flood prediction. Field observations show that TWL methods perform poorly, resulting in extensive over or under-prediction. All temporally variable overtopping model results were superior to static methods.

XBeach is often applied in a single deterministic run (e.g., Barnard et al., 2014; Stockdon et al., 2014), however random realizations showed significant runup and overtopping variability within each group of 10 runs. Boundary depth also significantly affected runup and overtopping rates. Both random realizations and appropriate offshore boundary depths for expected wave numbers must be considered.

**Table 5**  
Overtopping source location results summary. Fit statistics, flooded area, average predicted flood depths (standard deviation in parenthesis) and maximum predicted flood depths are shown.

Trial	$\Delta$ longshore	Cross-shore location	Points	$F_A$	$F_{OP}$	$F_{UP}$	$A$ ( $m^2$ )	$h_{avg}$	$h_{max}$
1	5	Landward crest	46	0.60	0.09	0.31	2007	5.56(4.02)	17.9
2	5	2 grid cells landward	46	0.71	0.15	0.14	2674	6.90(3.74)	18.9
3	5	Between crest/low	46	0.71	0.15	0.14	2677	6.90(3.76)	19.0
4	5	Back beach low	46	0.71	0.15	0.14	2723	7.38(3.83)	19.1
5	10	Between crest/low	23	0.71	0.15	0.14	2675	6.78(3.85)	19.3
6	15	Between crest/low	15	0.71	0.15	0.14	2689	6.97(3.88)	19.2
7	20	Between crest/low	11	0.71	0.15	0.14	2672	6.78(3.82)	19.2
8	30	Between crest/low	8	0.71	0.15	0.14	2693	6.89(4.03)	19.9
9	40	Between crest/low	5	0.71	0.15	0.14	2717	7.54(3.84)	18.7
10	~ 80	Between crest/low	3	0.69	0.23	0.08	3201	10.1(5.29)	22.3
11	~ 80	Back beach low	3	0.65	0.31	0.04	3672	14.4(9.30)	63.0

Accurate beach and back-beach topographic characterization is crucial in rapidly variable, densely built coastal areas. Local beach depressions retained and infiltrated overtopped flows. The bare earth DEM oversmoothed high elevations where structures were removed. In this case, terrain changes could be observed in Google Earth and alternative LiDAR data was available to supplant the problematic region. Accurate urban coastal flood modeling often requires site specific knowledge and topographic data.

Wave overtopping field observations are exceedingly rare and validation data paucity inhibits accurate urban coastal flood modeling and prediction. This study benefits from flood extent observations; however, depth, velocity field and overflow measurements are needed to rigorously validate impulsively driven overtopping flows and advance coastal flood modeling.

## Acknowledgments

This work was supported by the University of California, San Diego Chancellor's Fellowship, California Department of Parks and Recreation, Division of Boating and Waterways Oceanography Program (program manager R. Flick) and the United States Army Corps of Engineers. Brian Woodward, Kent Smith, Dennis Darnell, Bill Boyd and Rob Grenzeback collected beach and bathymetry data used in this work. Sean Crosby provided MEM CDIP wave spectra. The author would like to thank the three reviewers for their constructive comments that strengthened this manuscript.

## References

- Anselme, B., Durand, P., Thomas, Y.F., Nicolae-Lerma, A., 2011. Storm extreme levels and coastal flood hazards: a parametric approach on the french coast of languedoc (district of leucate). *Compt. Rendus Geosci.* 343, 677–690.
- Barnard, P.L., van Ormondt, M., Erickson, L.H., Eshleman, J., Hapke, C., Ruggiero, P., Adams, P.N., Foxgrover, A.C., 2014. Development of the coastal storm modeling system (CoSMoS) for predicting the impact of storms on high-energy active-margin coasts. *Nat. Hazards* 74 (2), 1095–1125.
- Bates, P.D., Dawson, R.J., Hall, J.W., Horritt, M.S., Nicholls, R.J., Wicks, J., Hassan, M.A.A.M., 2005. Simplified two-dimensional numerical modelling of coastal flooding and example applications. *52* (9), 793–810.
- Battjes, J.A., Gerritsen, H., 2002. Coastal modelling for flood defence. *Phil. Trans. R. Soc. A* 360, 1461–1475.
- Bernatchez, P., Fraser, C., Lefavre, D., Dugas, S., 2011. Integrating anthropogenic factors, geomorphological indicators and local knowledge in the analysis of coastal flooding and erosion hazards. *Ocean Coast. Manag.* 53, 621–632.
- Booij, N., Ris, R.C., Holthuijsen, L.H., 1999. A third generation wave model for coastal regions: 1. Model description and validation. *J. Geophys. Res. Oceans* (1978–2012) 104 (C4), 7649–7666.
- Brown, J.D., Spencer, T., Moeller, I., 2007. Modeling storm surge flooding of an urban area with particular reference to modeling uncertainties: a case study of Canvey Island, United Kingdom. *Water Resour. Res.* 43 (W06402), <http://dx.doi.org/10.1029/2005WR004597>.
- Carignan, K.S., Taylor, L.A., Eakins, B.W., Friday, D.Z., Grothe, P.R., Love, M., 2012. Digital Elevation Models of San Diego, California: Procedures, Data Sources and Analysis. NOAA National Geophysical Data Center Technical Report, Boulder, CO 32.
- Cheung, K.F., Phadke, A.C., Wei, Y., Rojas, R., Douyere, Y.J.M., Martino, C.D., Houston, S.H., Liu, P.L.F., Lynett, P.J., Dodd, N., Liao, S., Nakazaki, E., 2003. Modeling of storm induced coastal flooding for emergency management. *Ocean Eng.* 30, 1353–1386.
- Church, J.A., Clark, P.U., Cazenave, A., Church, J.A., Church, J.A., Gregory, J.M., Jevrejeva, S., Levermann, A., Merrifield, M.A., Milne, G.A., Nerem, R.S., Nunn, P.D., Payne, A.J., Pfeffer, W.T., Stammer, D., Unnikrishnan, A.S., 2013. Sea level change. In: Stocker, T.F., Qin, D., Plattner, G.-K., Tignor, M., Allen, S.K., Boschung, J., Nauels, A., Xia, Y., Bex, V., Midgley, P.M. (Eds.), *Climate Change 2013: The Physical Science Basis, Contribution of Working Group I to the Fifth Assessment Report of the Intergovernmental Panel on Climate Change*. Cambridge University Press, Cambridge, UK, New York, NY, USA, pp. 1137–1216.
- Climate Central, 2015. Surging seas, sea level rise analysis by Climate Central. Accessed May 5, 2015 at: <http://sealevel.climatecentral.org/>.
- Dawson, R.J., Dickson, M.E., Nicholls, R.J., Hall, J.W., Walkden, M.J.A., Stansby, P., Mokrech, M., Richards, J., Zhou, J., Milligan, J., Jordan, A., Pearson, S., Rees, J., Bates, P., Koukoulas, S., Watkinson, A., 2009. Integrated analysis of risks of coastal flooding and cliff erosion under scenarios of long term change. *Clim. Chang.* 95 (1–2), 249–288.
- Federal Emergency Management Agency (FEMA), 2004. Guidelines and specifications for flood hazard mapping partners appendix D. Final draft guidelines for coastal flood hazard analysis and mapping for the Pacific Coast of the United States. Available online at: <http://www.fema.gov/library/viewRecord.do?id=2188>.
- Flick, R., Murray, J., Ewing, L., 2003. Trends in United States tidal datum statistics and tide range. *J. Waterway, port, coastal, Ocean Eng.* 129 (4), 155–164.
- Gallien, T.W., Barnard, P., van Ormondt, M., Foxgrover, A., Sanders, B.F., 2012. A Parcel-scale coastal flood forecasting prototype for a Southern California urbanized embayment. *J. Coast. Res.* 31, 47–60.
- Gallien, T.W., Schubert, J., Sanders, B.F., 2011. Predicting tidal flooding of urbanized embayments: a modeling framework and data requirements. *Coast. Eng.* 58 (6), 567–577.
- Gallien, T.W., Sanders, B.F., Flick, R.E., 2014. Urban coastal flood prediction: integrating wave overtopping, flood defenses and drainage. *Coast. Eng.* 91, 18–28.
- Heberger, M., Cooley, H., Herrera, P., Gleick, P.H., Moore, E., 2009. The Impacts of Sea-Level Rise on the California Coast. California Climate Change Center, Sacramento.
- Hubbard, M.E., Dodd, N., 2002. A 2D numerical model of wave run-up and overtopping. *Coast. Eng.* 47, 1–26.
- Hunt, J.C.R., 2005. Inland and coastal flooding: developments in prediction and prevention. *Phil. Trans. R. Soc. A* 363, 1475–1491.
- Hunter, J., 2012. A simple technique for estimating an allowance for uncertain sea-level rise. *Clim. Chang.* 113, 239–252.
- Knowles, N., 2009. Potential Inundation Due to Rising Sea Levels in the San Francisco Bay Region. California Climate Change Center, Sacramento.
- Laudier, N.A., Thornton, E.B., MacMahan, J., 2011. Measured and modeled wave overtopping on a natural beach. *Coast. Eng.* 58, 815–825.
- Le Roy, S., Pedreros, R., Andr, C., Paris, F., Lecacheux, S., Marche, F., Vinchon, C., 2014. Coastal flooding of urban areas by overtopping: dynamic modelling application to the Johanna storm (2008) in Gávres (France). *Nat. Hazards Earth Syst. Sci. Discuss.* 2 (8), 4947–4985.
- Ludka, B.C., Guza, R.T., O'Reilly, W.C., 2015. Observations of Four Nourished Beaches. *Coastal Sediments 2015*, San Diego, CA.
- Lynett, P.J., Melby, J.A., Kim, D.H., 2010. An application of Boussinesq modeling to hurricane wave overtopping and inundation. *Ocean Eng.* 37 (1), 135–153.
- Martinelli, L., Zanuttigh, B., Corbau, C., 2010. Assessment of coastal flooding hazard along the Emilia Romagna littoral, IT. *Coast. Eng.* 57, 1042–1058.
- Mawdsley, R.J., Haigh, I.D., Wells, N.C., 2015. Global secular changes in different high water, low water and range levels. *Earth's Future* 3, 66–81.
- McCall, R., Thiel de Vries, J.S.M., Van, Plant, N.G., Van Dongeren, A.R., Roelvink, J.A., Thompson, D.M., Reniers, A.J.H.M., 2010. Two-dimensional time dependent hurricane overwash and erosion modeling at Santa Rosa Island. *Coast. Eng.* 57, 668–683.
- McCall, R., 2013. Xbeach forum. Available at: [http://oss.deltares.nl/web/xbeach/forum/-/message\\_boards/view\\_message/230649](http://oss.deltares.nl/web/xbeach/forum/-/message_boards/view_message/230649).
- Nicholls, R.J., 2010. Impacts of and responses to sea-level rise. *Understanding Sea-Level Rise and Variability*. Wiley-Blackwell, Chichester, UK.
- National Oceanic and Atmospheric Administration (NOAA), 2015. Sea level rise and coastal flooding impacts. Accessed May 5, 2015 at: <http://coast.noaa.gov/slr/>.
- Poulter, B., Halpin, P.N., 2008. Raster modelling of coastal flooding from sea-level rise. *Int. J. Geogr. Inf. Sci.* 22 (2), 167–182.
- Prime, T., Brown, J.M., Plater, A.J., 2015. Physical and economic impacts of sea-level rise and low probability flooding events on coastal communities. *PLoS ONE* 10(2) e0117030, <http://dx.doi.org/10.1371/journal.pone.0117030>.
- Pullen, T., Allsop, N.W.H., Bruce, T., Kortenhuis, A., Schüttrumpf, H., Van der Meer, J.W., 2007. *EuroTop: Wave Overtopping of Sea Defences and Related Structures: Assessment Manual*. Available at: <http://www.overtopping-manual.com/manual.html>.
- Purvis, M.J., Bates, P.D., Hayes, C.M., 2008. A probabilistic methodology to simulate future coastal flood risk due to sea level rise. *Coast. Eng.* 55, 1062–1073.
- Reeve, D.E., Soliman, A., Lin, P.Z., 2008. Numerical study of combined overflow and wave overtopping over a smooth impermeable seawall. *Coast. Eng.* 55, 155–166.
- Roelvink, D., Reniers, A., Van Dongeren, A., van Thiel de Vries, J., McCall, R., Lescinski, J., 2009. Modelling storm impacts on beaches, dunes and barrier islands. *Coast. Eng.* 56, 1133–1152.
- Sanders, B.F., 2007. Evaluation of on-line DEMs for flood inundation modeling. *Adv. Water Resour.* 30 (8), 1831–1843.
- Shewchuk, J.R., 1996. Triangle: engineering a 2D quality mesh generator and Delaunay triangulator in: applied computational geometry: towards geometric engineering. In: Lin, M.C., Manocha, D., *Lecture Notes in Computer Science*, vol 1148. springer-verlag. pp. 203–222. Software: <http://www-2.cs.cmu.edu/~quake/triangle.html>.
- Smit, P., Stelling, G., Roelvink, J.A., Van Thiel de Vries, J.S.M., McCall, R.T., Van Dongeren, A.R., Zwinkels, C., Jacobs, R., 2010. XBeach: Non-Hydrostatic Model: Validation, Verification and Model Description. Technical report. Delft University of Technology.
- Smith, R.A.E., Bates, P.D., Hayes, C., 2012. Evaluation of a coastal flood inundation model using hard and soft data. *Environ. Model. Softw.* 30, 35–46.
- Splinter, K.D., Palmsten, M.L., 2012. Modeling dune response to an east coast low. *Mar. Geol.* 329331, 46–57.
- Stockdon, H.F., Thompson, D.M., Plant, N.G., Long, J.W., 2014. Evaluation of wave runup predictions from numerical and parametric models. *Coast. Eng.* 92, 1–11.
- Stockdon, H.F., Holman, R.A., Howd, P.A., Sallenger, A.H., 2006. Empirical parameterization of setup, swash and runup. *Coast. Eng.* 53, 573–588.
- Sweet, W.V., Park, J., 2014. From the extreme to the mean: acceleration and tipping points of coastal inundation from sea level rise. *Earth's Future* 2, 1–11.
- TAW, 2002. Technical report wave run-up and wave overtopping at dikes. Technical Advisory Committee on Flood Defence, The Netherlands.

- Taylor, Peter J., 1977. *Quantitative Methods in Geography: An Introduction to Spatial Analysis*. Houghton Mifflin Harcourt, Boston, Massachusetts., pp. 396
- Tebaldi, C., Strauss, B.H., Zervas, C.E., 2012. Modelling sea level rise impacts on storm surges along US coasts. *Environ. Res. Lett.* 7, 12
- Tsubaki, R., Fujita, I., 2010. Unstructured grid generation using LiDAR data for urban flood inundation modeling. *Hydrol. Process.* 24, 1404–1420.
- Wadey, M.P., Nicholls, R.J., Hutton, C., 2012. Coastal flooding in the solent: An integrated analysis of defences and inundation. *Water* 4, 430–459.
- Zijlema, M., Stelling, G.S., 2008. Efficient computation of surf zone waves using the nonlinear shallow water equations with non-hydrostatic pressure. *Coast. Eng.* 55 (10), 780–790.